

Stability of antiferroelectricity and molecular reorientation in the hexatic smectic I_A^* phase as studied by X-ray diffraction and NMR spectroscopy

Yoichi Takanishi,^{a*} Kouichi Miyachi,^a Shohei Yoshida,^a Bo Jin,^a Huiyong Yin,^a Ken Ishikawa,^a Hideo Takezoe,^a and Atsuo Fukuda^b

^aDepartment of Organic and Polymeric Materials, Tokyo Institute of Technology, O-okayama, Meguro-ku, Tokyo 152-8552, Japan

^bDepartment of Kansei Engineering, Shinshu University, Ueda-shi, Nagano-ken 386-8567, Japan

We have investigated molecular orientation in the hexatic antiferroelectric SI_A^* phase by X-ray diffraction and nuclear magnetic resonance (NMR) spectroscopy. In the phase transition from SC_A^* to SI_A^* , the layer thickness increases and becomes larger than that in SA. The third-order diffraction peak intensity becomes stronger than the second-order one at this transition and increases with decreasing temperature in SI_A^* . According to the magic angle spinning NMR measurements, on the other hand, the isotropic chemical shift scarcely moves at this transition. These results suggest that the layer structure is reconstructed by the molecular reorientation but not by a molecular conformation change. We have also discussed the stability of antiferroelectricity and the origin of its appearance in hexatic ordering.

Smectic liquid crystals have a variety of phase sequences. In particular, the discovery of the antiferroelectric liquid crystal (AFLC) phase makes the system more complex, attracting much research interest. One of the most interesting phenomena is the appearance of many subphases such as a ferroelectric SC_γ^* and a reentrant antiferroelectric AF phase² between the ferroelectric SC^* and antiferroelectric SC_A^* phases. This is called the 'devil's staircase',³ which appears to be due to the competition between ferroelectricity and antiferroelectricity. Yamashita⁴ adopted the axial next-nearest neighbor Ising spin (ANNNI) model as an explanation for this successive phase transition.

Also of interest is the occurrence of the hexatically ordered antiferroelectric phase.⁵ Fig. 1 shows the X-ray Laue pattern in a 100 μm thick freely suspended film, the optical transmittance spectrum of oblique incidence, and the electrooptic response showing the double hysteresis loop in the smectic phase just below SC_A^* in 4-(1-trifluoromethylheptyloxy-carbonyl)phenyl 4'-nonylcarbonyloxybiphenyl-4-carboxylate (TFMHPNCBC). These results indicate that this phase has both SI-like hexatic ordering and antiferroelectricity. Therefore, we call this phase SI_A^* . Although the normal ferroelectric hexatic SI^* phase has been studied,⁶ the origin of its appearance has not been clarified; less is known about the hexatic antiferroelectric phase. Neundorf *et al.*⁷ studied the binary systems of two AFLCs, and proposed a different intermolecular interaction from that stabilizing SC_A^* as a possible origin of the stabilization of SI_A^* . However, the suggestion has not yet been verified. Hence, it is important to consider the origin of antiferroelectricity in the hexatic smectics from the viewpoint not only of the relation between the intermolecular interactions producing hexatic ordering and antiferroelectric properties but also in the discussion of the origin of the antiferroelectric SC_A^* phase.

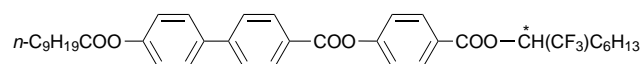
In this paper, we investigated molecular orientation in the SI_A^* phase in detail by X-ray diffraction and NMR spectroscopy. We measured the temperature dependence of the layer thickness, the higher-order diffraction intensity by X-ray diffraction and the isotropic chemical shift by NMR. In the X-

ray measurements, we found that the layer thickness increases at the phase transition from SC_A^* to SI_A^* and that the third-order peak intensity becomes larger than the second-order one. We also found that the isotropic chemical shift assigned to the chiral alkyl chain scarcely moves with temperature on the NMR timescale. These results do not suggest a molecular conformational change, but molecular reorientation within a layer at this transition. We also discuss the origin of the antiferroelectricity in hexatic smectics based on these experimental results.

Experimental

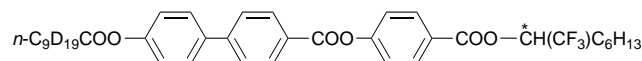
The compounds used were (R)-TFMHPNCBC and [²H₁₉]- (R)-TFMHPNCBC,⁸ whose chemical structure and the phase sequence (temperatures in °C) are as follows.

(R)-TFMHPNCBC



Iso 121–120.3 SA 107.0–106.8 SC_A^* 56–55 SI_A^* ~28 Cryst.

[²H₁₉]- (R)-TFMHPNCBC



Iso 120 SA 106 SC_A^* 55 SI_A^* ~28 Cryst.

The deuteration scarcely changed its phase sequence at each transition temperature.

In the X-ray measurements, we used a Rigaku RU-200 (Cu-K α , 12 kW) instrument with a temperature controller with an accuracy of ± 0.1 °C. A sample was stretched thin with a spatula just above the Iso-SA phase transition, so that it was uniformly and homeotropically aligned. The film thickness was *ca.* 25 μm . The temperature dependences of the layer thickness and the corresponding higher-order peaks were measured by the conventional 2θ - θ method.⁹ The apparent optical tilt angle, θ_{opt} , was determined by measuring the extinction direction in

* E-mail: ytakanis@o.cc.titech.ac.jp

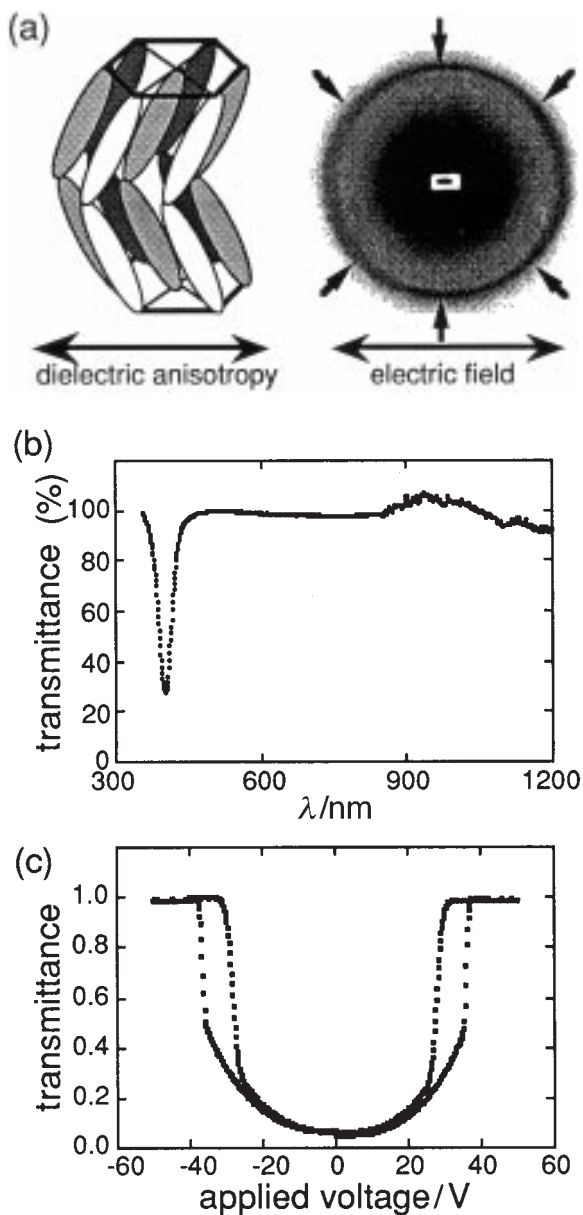


Fig. 1 Evidence for the hexatic antiferroelectricity in SI_A^* of TFMHPNCBC, (a) an X-ray Laue pattern in a $100\ \mu\text{m}$ thick freely suspended film (b) an optical transmittance spectrum of oblique incidence in a $50\ \mu\text{m}$ thick homeotropic cell, and (c) an optical transmittance change by applying a triangular wave electric field in a $2\ \mu\text{m}$ thick homogeneous cell

a $2\ \mu\text{m}$ thick homogeneously aligned cell between crossed polarizers when we applied a sufficiently high electric field to make the field induced phase transition to the ferroelectric state.

NMR spectroscopic measurements were performed with a Chemagnetics high resolution solid NMR spectrometer CMX-300WB (300 MHz for ^1H). Isotropic chemical shifts at each carbon were measured by magic angle spinning (MAS) with and without cross-polarization (CP). The 90° pulse width was $2.4\ \mu\text{s}$, and the contact time was $5\ \text{ms}$ in the CP method. The sample rotation frequency was $4\ \text{kHz}$. The samples were packed into a zirconia tube of diameter $7\ \text{mm}$. We started the NMR measurements after $10\ \text{min}$ to obtain thermal equilibration at each temperature. Although each temperature was stabilized by using VT (variable temperature) air to within $\pm 1^\circ\text{C}$ accuracy, the absolute value of the sample temperature was different from the set value. The temperature was calibrated by finding the temperature at which a free induction decay

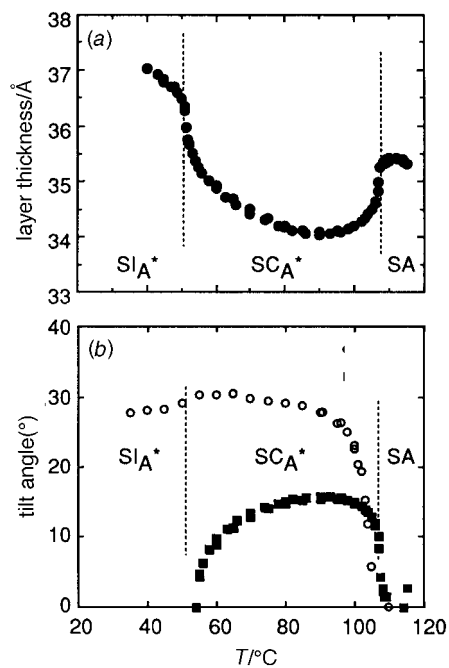


Fig. 2 (a) Temperature dependence of the layer thickness of (R)-TFMHPNCBC and (b) temperature dependence of (○) the apparent optical tilt angle, θ_{opt} , and (■) the tilt angle determined by X-ray, $\theta_{\text{X-ray}}$

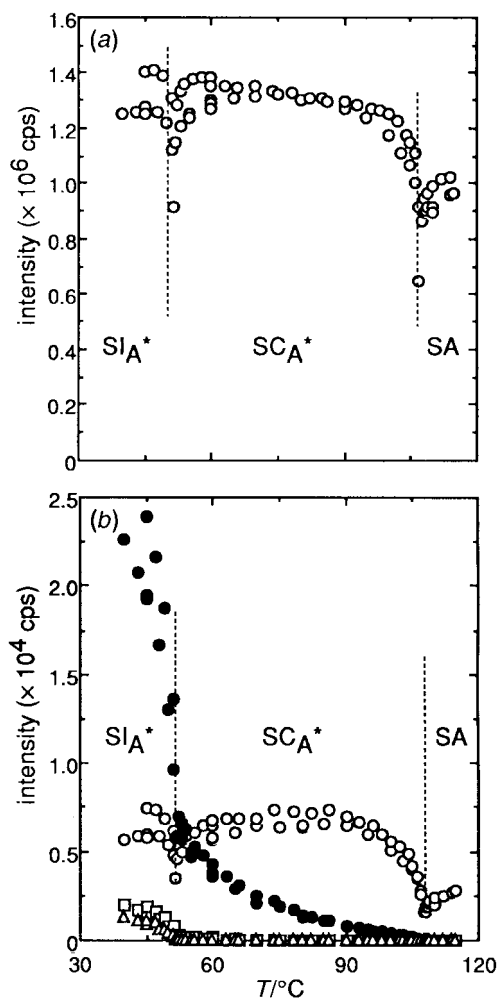


Fig. 3 Temperature dependences of (a) the first- and (b) higher-order peak intensities of the X-ray diffraction peak due to the layer spacing (○) 2nd-order (●) 3rd-order (□) 4th-order and (△) 5th-order

(FID) signal drastically changes; note that a FID signal shows a long decay in the isotropic liquid state.

Results and Discussion

X-Ray studies

Fig. 2(a) shows the temperature dependence of the layer thickness of (*R*)-TFMHPNCBC. At the phase transition from SA to SC_A^{*}, the layer thickness decreases because of molecular tilting from the layer normal. With a decrease in temperature

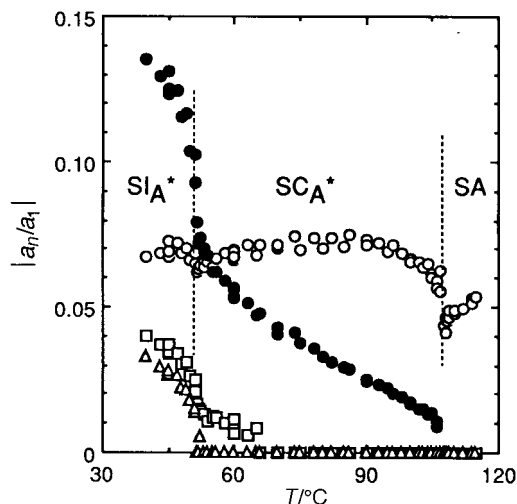


Fig. 4 Temperature dependences of the normalized amplitudes of the higher-order diffraction, $|a_n/a_1|$: (○) a_2/a_1 , (●) a_3/a_1 , (□) a_4/a_1 , and (△) a_5/a_1

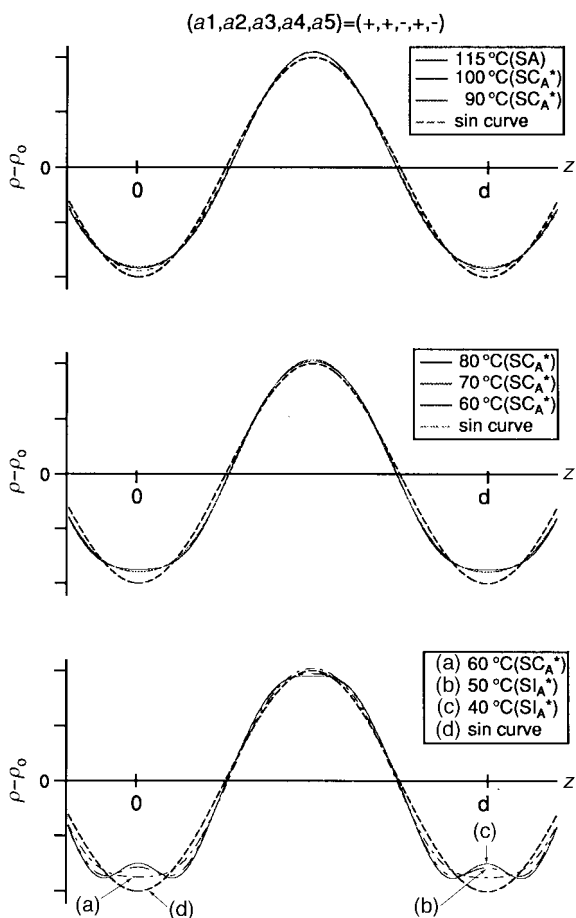


Fig. 5 Density projection profiles along the layer normal, z , in the SA, SC_A^{*} and SI_A^{*} phases determined by the results of Fig. 4

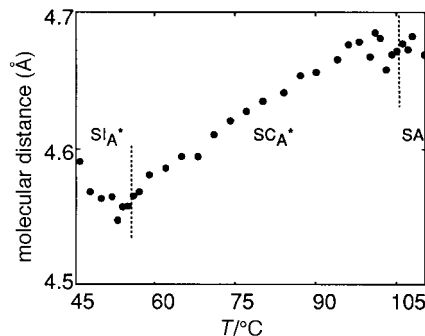


Fig. 6 Temperature dependence of the in-plane molecular distance determined by a wide angle X-ray diffraction peak

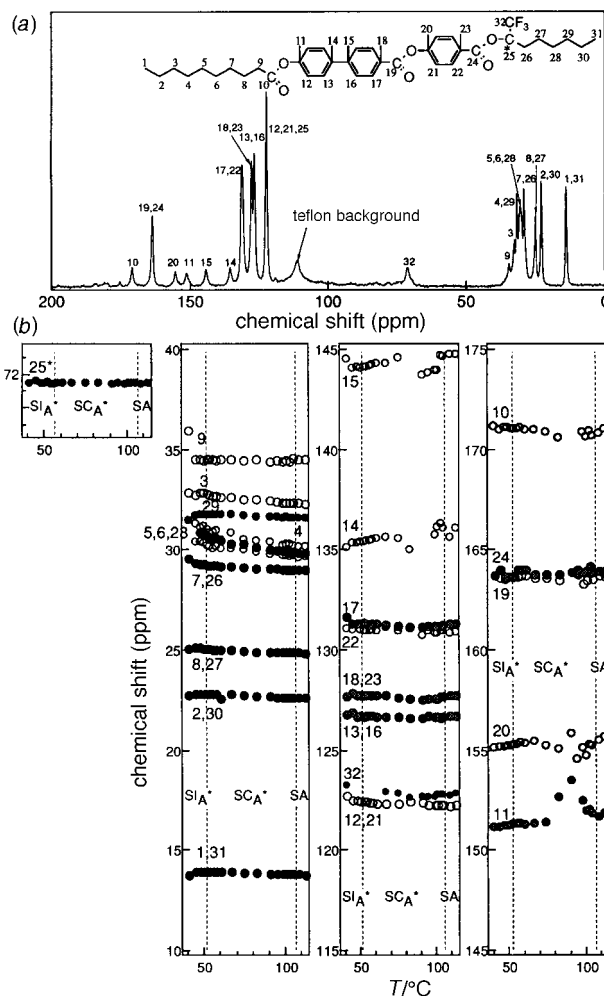


Fig. 7 (a) Typical CP-MAS spectrum in SA of TFMHPNCBC, and (b) the temperature dependence of the isotropic chemical shift. The assigned number in Fig. 7(b) corresponds to the number in the chemical structure shown above

in SC_A^{*}, the layer shrinkage saturates at about 90 °C, and the layer thickness begins to increase at the far lower temperature region in SC_A^{*}. The layer thickness steeply increases at the transition from SC_A^{*} to SI_A^{*}, and to our surprise, it becomes longer than that in the SA phase. On the other hand, the apparent optical tilt angle, θ_{opt} , continuously increases in the temperature region of the SC_A^{*} phase, and it only decreases slightly at the SC_A^{*}-SI_A^{*} phase transition, as shown in Fig. 2(b). In Fig. 2(b), the tilt angle, θ_{x-ray} , given by eqn. (1),¹⁰

$$\theta_{x-ray}(T) = \cos^{-1}[d(T)/d_A] \quad (1)$$

is also shown as a function of temperature. Here, $d(T)$ is the layer thickness in the SC_A^{*} and SI_A^{*}, and d_A is that in the SA

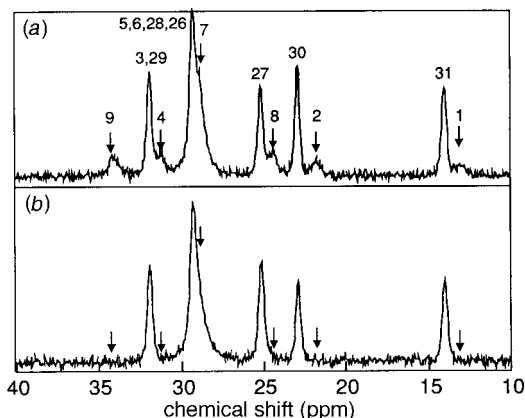


Fig. 8 ^{13}C NMR spectra of the alkyl chain region of $[\text{2H}_{19}]$ -TFMHPNCBC in the MAS measurement (a) without and (b) with CP

phase at 110°C , determined by the X-ray measurements. The temperature dependence of $\theta_{\text{x-ray}}$ is clearly different from that of θ_{opt} . By taking into account the fact that θ_{opt} and $\theta_{\text{x-ray}}$ are governed by the tilting of the core part of the molecules and that of the average long molecular axis, respectively, the different θ could be attributed to molecular conformational change and/or the change of the molecular interdigitation in a smectic layer.

In order to study the layer structure in detail, we measured the higher-order Bragg peaks corresponding to the layer thickness.⁹ Fig. 3 shows the temperature dependence of the higher-order peak intensities. The first- and second-order peaks decrease at the $\text{SA}-\text{SC}_A^*$ and $\text{SC}_A^*-\text{SI}_A^*$ phase transitions, indicating the occurrence of molecular reorientation. In the SI_A^* phase, even a fifth-order peak was detected. In the vicinity of the $\text{SC}_A^*-\text{SI}_A^*$ phase transition, the third-order peak does

not show any decrease, and becomes larger than the second-order one. These results qualitatively indicate that the smectic layer order is very high compared with that of other fluid smectic phases of low molecular weight compounds.

We consider the projection of the electron density along the layer normal, $\rho(z)$. The smectic layer is symmetric with respect to the layer normal because of the head-and-tail equivalence of the molecule, $\rho(z) = \rho(-z)$. Since $\rho(z)$ is a periodic function of the layer thickness, d , it may be expanded as a Fourier series as given by eqn. (2).

$$\rho(z) = \rho_0(z) + \sum a_n \cos(2\pi n z d)^{11} \quad (2)$$

The absolute values of the coefficients $|a_n|$ can be obtained by the higher-order peak intensities corresponding to the layer thickness after making a correction for Lorentz factors. The normalized amplitudes of the higher-order diffractions, $|a_n/a_1|$ ($n=2-5$), are shown as a function of temperature in Fig. 4. Based on this figure, we depicted the density projection profile along the layer normal at each phase in Fig. 5. For the calculation we chose the signs of a_1, a_2, a_3, a_4, a_5 as $+, +, -, +, -$ on the basis of the bent molecular structure and the molecular reorientation at the $\text{SC}_A^*-\text{SI}_A^*$ phase transition, which is discussed below. In the SA phase and the higher temperature region of SC_A^* , the density profiles are similar to the sinusoidal wave-form, although $|a_2/a_1|$ and $|a_3/a_1|$ are much larger than that in the normal smectic liquid crystals such as 8CB.¹² In contrast, the profile is separate from the sinusoidal wave in the lower temperature region of SC_A^* , and a substructure arises at the layer boundaries in SI_A^* .

Fig. 6 shows the temperature dependence of the in-plane molecular distance obtained by wide angle X-ray diffraction. In the temperature region of SC_A^* , the distance gradually decreases with a decrease in temperature. It indicates that the fluctuation of the molecule is gradually hindered and molecular order in the layer increases. At the transition from SC_A^* to

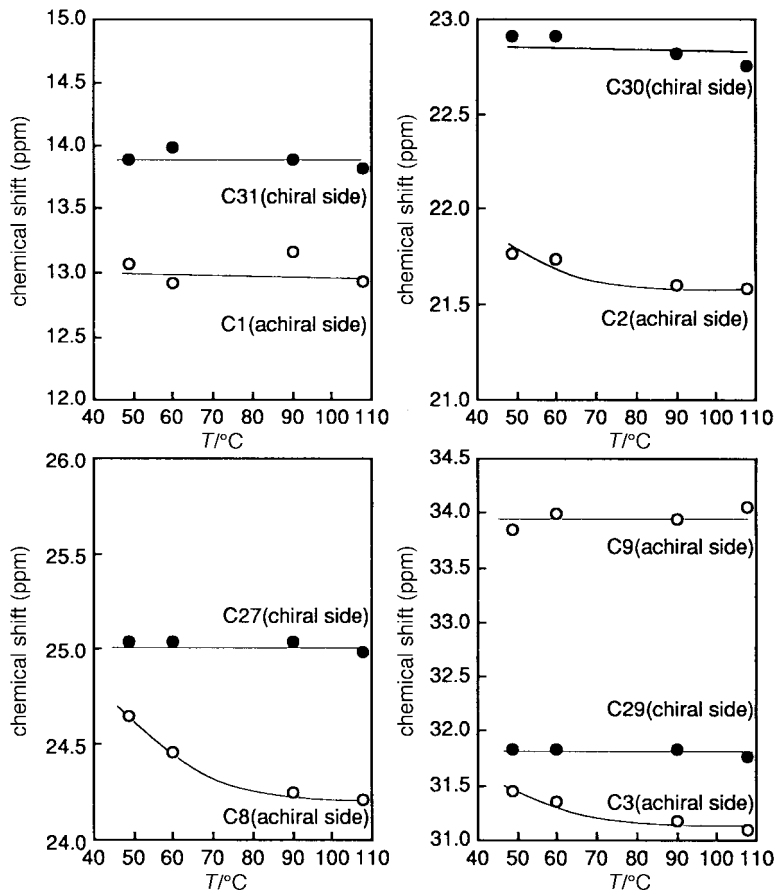


Fig. 9 Temperature dependences of the chemical shift corresponding to the alkyl carbons

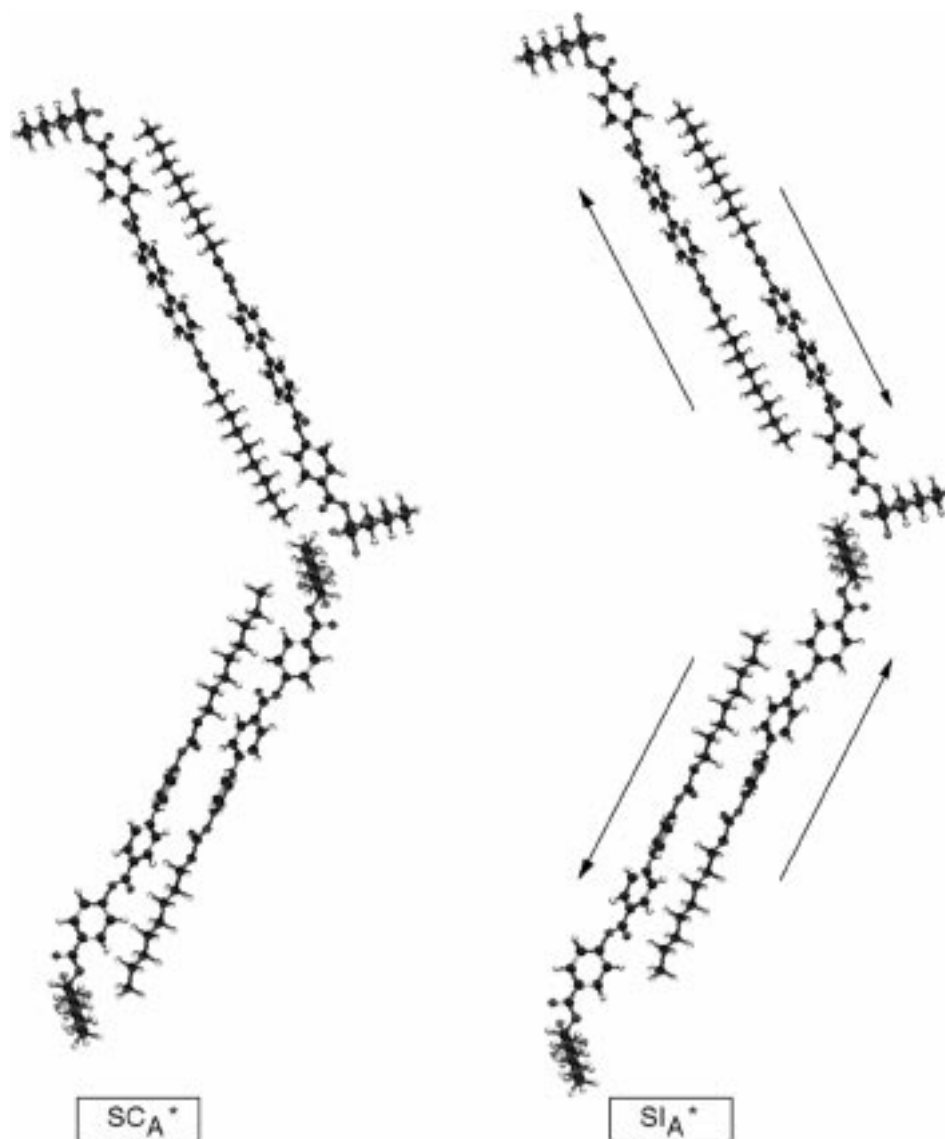


Fig. 10 Schematic illustration of the model structure at the phase transition from SC_A^* to SI_A^* . The result in the MOPAC calculation was adopted as the molecular shape. Bend type molecular length: $L_0 = 33.829$ Å; layer thickness in SA (112 °C): $d_A = 35.429$ Å; layer thickness in SI_A^* (40 °C): $d_{IA} = 37.015$ Å; apparent tilt angle in SI_A^* (40 °C): $\theta_{opt} = 28.15^\circ$. Supposing that $L = d/\cos\theta_{opt}$, $L_A(112^\circ\text{C}) = d_A = 35.429$ Å, $L_{IA}(40^\circ\text{C}) = 41.9806$ Å (L = the average length along the molecular long axis). Then SA: $L_A - L_0 = 1.6$ Å and SI_A^* : $L_{IA} - L_0 = 8.1516$ Å. The difference of interdigitation is estimated to be about 6.55 Å.

SI_A^* , the molecular distance starts increasing. If the molecular conformation change to an elongated form at the transition causes the thickness of the layer to increase, the molecular distance within each layer should also exhibit a significant change. Therefore, the increasing layer thickness at this transition is thought to be caused by a change in molecular interdigitation but not by a large change in conformation.

NMR studies

In order to investigate the molecular conformation in detail, NMR measurements were performed. Fig. 7(a) and 7(b) show a typical CP-MAS spectrum in SA of (*R*)-TFMHPNCBC and the temperature dependence of the isotropic chemical shift, respectively. The assigned number of each carbon is indicated on the figure. With decreasing temperature in the SC_A^* phase, the peak intensities corresponding to the chemical shifts assigned to the phenyl carbons (C11, C14, C15 and C20) decrease and move up field. The decrease in intensity indicates the slow movement of the molecules, and the low-field shift suggests a change in the dihedral angle at the corresponding position. The peaks assigned to the ester carbons (C10, C19, C24) become broad and in particular the peaks assigned to

C19 and C24 appear to coalesce. Yoshizawa *et al.*¹³ reported that line broadening occurs when $\omega_1\tau \approx 1$, where ω_1 corresponds to the proton decoupling power and τ is the correlation time of the molecular motion. If this is the case, the present result indicates the reorientation of molecules in a layer. The temperature at which this line broadening occurs is almost the same as the temperature at which $\theta_{x\text{-ray}}$ saturates (around 90 °C). In addition, the chemical shifts of the phenyl carbons connected to the carbons of the ester groups, C18 and C23, and ester carbons, C19 and C24, hardly move in the temperature range, suggesting that the angle between the dipole of the ester and the phenyl plane connected to them remains unchanged. In contrast, the chemical shift assigned to some alkyl carbons moves to lower field in the vicinity of the transition from SC_A^* to SI_A^* .

In order to distinguish between the peaks corresponding to the alkyl carbons of the achiral and chiral sides, $[^2\text{H}_{19}]$ -(*R*)-TFMHPNCBC was used. Fig. 8 shows a part of the MAS spectrum of $[^2\text{H}_{19}]$ -(*R*)-TFMHPNCBC with and without CP. Some peaks exhibit up field shifts in the MAS measurement (no CP) while these peaks disappear with CP. The upfield shift is caused by the dipolar coupling with deuteriums, and thus we could distinguish between chiral and achiral alkyl chains.

The temperature dependence of the chemical shifts corresponding to some of the alkyl carbons is shown in Fig. 9. The peaks assigned to the achiral carbons, with the exception of C9, shift slightly to lower field with decreasing temperature, while the chiral carbon peaks do not move. Ishikawa and Ando¹⁴ reported that the ¹³C chemical shift moves to lower field if a carbon atom three-bonds distant is *trans* rather than *gauche*. Therefore, this low-field shift may indicate a conformational change of the achiral alkyl chain. Benattar *et al.*¹⁵ explained that the increase in layer thickness at the transition from SC* to the hexatic SI* phase is caused by an increase in the orientational order of an alkyl chain. In the present case, the layer thickness in SI_A* in which the long molecular axis tilts with respect to the layer normal by 30° is larger than that in the SA phase. Hence the layer thickness change is too large to be explained by only an increase in the alkyl chain orientational ordering. Therefore, the main cause of the layer thickness change, we suggest, is the change in molecular interdigitation due to intralayer molecular reorientation, though the conformational change of the achiral chain may influence the pretransitional phenomenon of the appearance of hexatic ordering. These results are also consistent with the polarized FT-IR results of Yin *et al.*,⁸ even in the SI_A* phase, the chiral chain is bent and the angle between the long molecular axis and the average chiral chain axis is much larger, as observed in MHPOBC and reported by Nakai *et al.*,¹⁶ Jin *et al.*¹⁷ and Ouchi *et al.*¹⁸

Let us consider the origin of the antiferroelectricity in the hexatically ordered smectic phase. Neundorf *et al.*⁷ assumed that the layer increase is due to a conformational change and proposed that it is probable that the Coulomb interaction through polarization changes due to positional fluctuations inherent in the hexatic order causes the SI_A* antiferroelectricity. However, the assumption, *i.e.* a significant molecular conformation change is the cause, is not correct as we have shown by NMR in this paper. Since the hexatic phases are a commonly observed phase in non-tilted and tilted smectic phases, the stabilization of SI_A* can naturally be considered to have the same origin as that of SC_A*, *i.e.* the so-called Px model¹⁹ or the pairing model.²⁰ In both models, intermolecular interactions at the layer boundary are important. If we consider the unchanged chemical shift, the increase of the layer thickness and electron density change at the SC_A*–SI_A* phase transition, the origin of the antiferroelectricity in hexatic SI_A* should be the same as in SC_A*; the electric interaction in the vicinity of layer boundaries. Therefore, we can conclude that the increase of layer thickness at this transition is caused by a molecular interdigitation change, which keeps the interlayer dipole interaction, so stabilizing the antiferroelectricity, which may be accompanied by an increase in the orientational order of the alkyl chains. We propose a model of molecular reorientation at the phase transition from SC_A* to SI_A* in Fig. 10.

Now, we have to give a reasonable explanation for the appearance of SI* below SC_A* or SI_A* as discovered by Neundorf *et al.*⁷ The key to the explanation is the temperature dependence of the layer spacing. The layer spacing shows a typical increase after the SC_A*–SI_A* phase transition as shown in Fig. 2(a) and in ref. 5 and 7. This may be due to the reduction of the interdigitation of molecules caused by the highly ordered smectic layer compared with that of the fluid smectic phases. As the layer becomes well ordered and the spacing gets thicker, the dipole–dipole interaction becomes weak. Then SI* emerges. This happens within the SI_A* phase (SI_A*–SI*) or at the phase transition from SC_A* to a hexatic phase (SC_A*–SI*) depending on the strength of the dipole–dipole interaction. Both transition sequences were observed in a mixture system.⁷

Considering that the ferroelectric SI* phase appears at a lower temperature than the antiferroelectric SI_A* phase, it is

difficult to propose that the excluded volume effect is the origin of the appearance of the hexatic phase in which molecules tilt in the same direction in neighboring layers such as SI(*). Therefore, dispersion forces may be the cause. At the phase transition from SC_A* to the hexatic phase at lower temperature, the competition between dipole–dipole interactions stabilizing antiferroelectric ordering and the interaction stabilizing hexatic ordering such as dispersion forces is important. If the former interaction is stronger than the latter then the antiferroelectric SI_A* phase appears. In contrast, if the latter overcomes the former, the phase transition to SI* occurs.

Conclusions

The conformation and reorientation of TFMHPNCBC molecules were studied in the SC_A* and the SI_A* phases by X-ray diffraction and NMR spectroscopy. The layer thickness gradually increases in the lower temperature region of SC_A*, and becomes larger in SI_A* than in SA. Higher-order X-ray diffraction results and NMR spectroscopy strongly indicate that this layer thickness increase is caused by translational molecular reorientation within a layer and not by a conformational change. From these results, we claim that this translational reorientation is due to the strong dipole interaction between molecules in adjacent layers, suggesting that the origin of the antiferroelectric ordering in hexatic smectics is the same as that in SC_A*.

We are very grateful to Showa Shell Sekiyu K. K. for supplying (R)-TFMHPNCBC. This work was supported by a Grant-in-Aid for Scientific Research (Specially Promoted Research No. 06102005) from Monbusho.

References

- 1 J. Lee, A. D. L. Chandani, K. Itoh, Y. Ouchi, H. Takezoe and A. Fukuda, *Jpn. J. Appl. Phys.*, 1990, **29**, 1122.
- 2 N. Okabe, Y. Suzuki, I. Kawamura, T. Isozaki, H. Takezoe and A. Fukuda, *Jpn. J. Appl. Phys.*, 1992, **32**, L793.
- 3 T. Isozaki, T. Fujikawa, H. Takezoe, A. Fukuda, T. Hagiwara, Y. Suzuki and I. Kawamura, *Phys. Rev. B*, 1993, **48**, 13439.
- 4 M. Yamashita, *Ferroelectrics*, 1996, **181**, 201.
- 5 Y. Takanishi, H. Takezoe and A. Fukuda, *Ferroelectrics*, 1993, **149**, 135.
- 6 S. K. Prasad, G. G. Nair and S. Chandrasekhar, *J. Mater. Chem.*, 1995, **5**, 2253.
- 7 M. Neundorf, Y. Takanishi, A. Fukuda, S. Saito, K. Murashiro, T. Inukai and D. Demus, *J. Mater. Chem.*, 1995, **5**, 2221.
- 8 H. Yin, B. Jin, Y. Takanishi, K. Ishikawa, H. Takezoe, A. Fukuda and M. Kakimoto, *Mol. Cryst. Liq. Cryst.*, 1997, **303**, 285.
- 9 Y. Takanishi, A. Ikeda, H. Takezoe and A. Fukuda, *Phys. Rev. E*, 1995, **51**, 400.
- 10 T. P. Rieker, N. A. Clark, G. S. Smith, D. S. Parmar, E. B. Sirota and C. R. Safinya, *Phys. Rev. Lett.*, 1987, **59**, 2658.
- 11 P. Davidson and A. M. Levelut, *Liq. Cryst.*, 1992, **11**, 469.
- 12 J. W. Stamatoff, P. E. Cladis, D. Guillon, M. C. Cross, T. Bilash and P. Finn, *Phys. Rev. Lett.*, 1980, **44**, 1509.
- 13 A. Yoshizawa and H. Kikuzaki, *Ferroelectrics*, 1993, **147**, 447.
- 14 S. Ishikawa and I. Ando, *J. Mol. Struct.*, 1992, **271**, 57.
- 15 J. J. Benattar, F. Moussa and M. Lambert, *J. Chim. Phys. Phys. - Chim. Biol.*, 1983, **80**, 99.
- 16 T. Nakai, S. Miyajima, S. Yoshida, Y. Takanishi and A. Fukuda, submitted to *Phys. Rev. E*.
- 17 B. Jin, Z. Ling, K. Miyachi, Y. Takanishi, K. Ishikawa, H. Takezoe, A. Fukuda, M. Kakimoto and T. Kitazume, *Phys. Rev. E*, 1996, **53**, R4295.
- 18 Y. Ouchi, Y. Yoshioka, H. Ishii, K. Seki, M. Kitamura, R. Noyori, Y. Takanishi and I. Nishiyama, *J. Mater. Chem.*, 1995, **5**, 2221.
- 19 K. Miyachi, J. Matsushima, Y. Takanishi, K. Ishikawa, H. Takezoe and A. Fukuda, *Phys. Rev. E*, 1995, **52**, R2153.
- 20 Y. Takanishi, K. Hiraoka, V. K. Agrawal, H. Takezoe, A. Fukuda and M. Matsushita, *Jpn. J. Appl. Phys.*, 1991, **30**, 2023.

Paper 7/07920F; received 4th November, 1997